1-2-2019

Design and Optimization of an Ionizing-Radiation-Free Dental Imaging Scheme by Near Infrared Fluorescence

Thomas Hartzler
thartz2@lsu.edu

DESIGN AND OPTIMIZATION OF AN IONIZING-RADIATION-FREE DENTAL IMAGING SCHEME BY NEAR-INFRARED FLUORESCENCE

A Thesis

Submitted to the Graduate Faculty of the
Louisiana State University and
Agricultural and Mechanical College
in partial fulfillment of the
requirements for the degree of
Master of Science

in

The Department of Electrical & Computer Engineering

By
Thomas Hartzler
B.S., Mississippi State University, 2014
May 2019

Table of Contents

Abbreviations

American Dental Association	ADA
Biological Effects of Ionizing Radiation	BEIR
Bovine Serum Albumin	BSA
Buccal Background	BB
Computed Tomography	CT
Cone Beam Computed Tomography	CBCT
First Molars	M1
Second Molars	M2
Grays	Gy
Indocyanine Green	ICG
Intensity-Mean Difference	IMD
Left Molars	LM
Lingual Background	LB
Magnetic Resonance Imaging	MRI
Molar Regions	MR
Near Infrared	NIR
Odds Ratio	OR
Phosphate Buffered Saline	PBS
Postnatal Day	P
Radiation Exposure Induced Cancer	REIC
Right Molars	RM

Sievert	Sv
Three Dimension	3-D
Two Dimension	2-D
Ultrasound	US

Abstract

There is a global need for access to oral health care. Proper oral health care is necessary for physiological and psychological health, as well as social and economic issues. Major oral diseases that must be screened include caries, cracked teeth, and impacted molars. These diseases are screened and diagnosed using a variety of medical imaging methods, computed tomography (CT) X-ray being the most popular and efficient method. The challenges in screening with X-ray technology include financial and time cost as well as health risk, including radiation exposure induced cancer (REIC). This thesis summarizes research to explore the possibility of overcoming these challenges using indocyanine green (ICG) near infrared (NIR) fluorescent imaging. An NIR imaging system was developed to image unerupted and erupted molars on test rats injected with ICG. Rats were injected with ICG and imaged using a variety of methods. Results show that for both erupted and unerupted molars occlusal wide-field imaging could identify the molar regions, and endoscopic imaging could clearly identify molar morphology including crowns and cusps. Fluorescent intensity data was collected using a spectrometer and analyzed to determine the optimized imaging window for the NIR dental imaging system. Further experiments were conducted to test the system's imaging capability on rat molars treated with laser ablation treatment, and on human teeth. We are the first group to develop and test a cost and time efficient, safe, and real-time NIR-I fluorescent imaging system for *in-situ* dental imaging.

1. Introduction

Oral Health Care and Common Oral Diseases

There is a universal need for access to dental health care. A lack of access to dental health care causes a variety of adverse health and socioeconomic side effects. Some studies estimate that children with nursing caries weigh about 1 kg less than controls, and that in the USA dental problems cost 117,000 hours lost in school per 100,000 children [1]. Further research suggests that poor oral health is associated with heart disease, stroke, diabetes, pre-term births, and low-birth-weight infants. Access to dental health can help screen for other diseases such as immune deficiency disorders, microbial infections, and oral cancer [2]. These are some of the reasons the surgeon general warns that overall health and quality of life is not achievable without oral health, and they should not be interpreted as separate entities [3].

Despite the need for access to oral health care, many oral diseases are still common. The most prevalent among oral diseases is caries, commonly known as cavities. A 2015 estimate claimed that in 2010 35% of the global population suffered from caries in their permanent teeth, and 9 % of the global population suffered from caries in their deciduous or baby teeth. If left untreated, caries can affect school performance and productivity at work [4]. In some instances, a clinical examination is not efficient enough to diagnose caries. Hidden caries is a type of lesion that appears healthy when inspected by standard dental routine. Many dentists rely on X-ray radiographs to screen for and diagnose hidden caries [5].

Impacted tooth is another prevalent oral disease. An impacted molar occurs when a molar fails to erupt and obtain a normal functioning position. The term erupt roughly means a tooth emerges from the gum and assumes its normal functions position. This most commonly occurs in the third molars, the “wisdom teeth,” affecting around 73% of young adults. Impacted

molars are generally extracted surgically to prevent infection, carious lesions, cysts, tumors, and the destruction of adjacent teeth. Complications resulting from extraction include sensory nerve damage, dry sockets, and pain. Before extraction, the molar is assessed via a radiographic evaluation. The objective is to image root morphology, size of follicular sac, dentistry of surrounding molars, and nerve vessels [6].

Dental Imaging Methods

In order to provide the highest quality of care to each individual patient, The American Dental Association (ADA) recommends periodic dental imaging for patients. The recommended guidelines suggest that images be taken no less frequently than once every 24 – 36 months for adults, and as frequently as every 6 – 12 months for some children [7]. Dentists generally rely on X-ray technology and magnetic resonance imaging to meet these recommendations; CT X-ray being the most popular method, consisting of one-third of all radiographic medical imaging in western European countries [8, 9].

Magnetic resonance imaging (MRI) provides a safe and effective dental imaging method, albeit it does have some limitations. MRI works by realigning hydrogen atoms in the body with a strong magnetic field. A radio frequency pulse depolarizes the atoms and the machine detects energy released from the atom as they realign with the magnetic field. MRI is generally applied to image soft tissues such as the saliva glands, however a recent method known as SWeep Imaging with the Fourier Transform can simultaneously image both soft and hard tissues [10]. It has also been demonstrated that MRI is well suited when imaging impacted teeth in children and adults [11].

The major challenges using MRI in dental imaging include cost and interference by metal objects. Ferromagnetic metals can be moved by the strong imaging magnet, or cause interface

when creating the image. MRI may not be safe for patients with cardiac pacemakers and artificial heart valves [10]. Metal braces and fillings are not a safety hazard for patients but can disrupt the acquired images making them useless. Cost is a second challenge associated with MRI. In 2009 the prices of a Cone Beam Computed Tomography (CBCT) and dental MRI examination were compared at the University of Wuerzburg, Germany. A dental CBCT examination was 175€, a 15-minute dental MRI examination was 206€. These prices can vary widely from different clinics and countries, but MRI is generally more expensive when compared to conventional radiographic methods [11].

Due to its low cost and superior spatial resolution, X-ray radiography is the most popular method utilized in modern dental imaging. The idea is that radiographic images can quickly and easily supplement clinical examinations to reveal caries and other diseases. Modern X-rays can be classified as two-dimension (2-D) and three-dimension (3-D).

2-D images are collected via conventional radiographs. Images are taken through either periapical, bitewing, and occlusal projections. With a periapical radiograph, the film is placed parallel to the z-axis of the tooth, and the X-ray is directed at a right angle to the film and the imaged tooth. An occlusal image is an image of the x and y plane of the oral cavity and can be thought of as a birds-eyes view. Occlusal images are useful for detecting impacted teeth and foreign bodies in the ducts of sub-mandibular glands. With bite-wing imaging, the patient bites into a film to keep the film in place with the crowns of the teeth. Bite-wing X-rays are useful for detecting inter-proximal and secondary caries. Excluding exposure to ionizing radiation, the biggest challenge with 2-D radiographs is that they collected a 2-D image of a 3-D area which causes a loss of spatial information. 2-D images do not collect information on the buccal side of the teeth and overlaying structures can cause super-imposition [10].

CT imaging methods, such as CBCT, use a narrow X-ray beam to take multiple exposures around an object to create a 3-D image. CT is used to acquired multiple, non-superimposed cross-sectional images to image both soft and hard tissues. Computer software color-enhancement features can be used to filter through soft tissues such as dental follicle and show specific depths within the object as chosen by the operator [12]. CT is one of the best methods available for diagnosing impacted teeth, as it allows the surgeon to visualize anatomic structures near-by. CBCT is the most frequent imaging method used by dentists today. The biggest challenge using CBCT is exposure to ionizing radiation, which exposes the patient to 3-44 times the dose as typical 2-D radiology [10, 11].

Ionizing Radiation and Associated Health Risk

Radiation typically refers to energy that propagates from a source as an electromagnetic wave, such as radio waves or X-rays. In a broad sense, ionizing radiation is electromagnetic radiation with enough energy to remove an electron from its orbital, ionizing its atom. Living tissues are 70 – 90 % water by weight, so ionizing radiation is often assumed to be radiation with enough energy to ionize water. This includes any radiation that exposes cells to 1216 kJ/mol or 12.6 eV/mol. Radiation with enough energy to ionize water begins in the deep ultra violet spectrum and continues through higher frequencies. Radiation that ionizes water molecules is what causes biological changes in cells and creates a risk of radiation exposure induced cancer (REIC) and other health effects [13, 14].

To estimate the risk from exposure to ionizing radiation, the total energy absorbed per unit mass must be estimated. This is often referred to as the absorbed dose. The SI unit for absorbed dose is the Gray (Gy), which is equivalent to $6.24 * 10^{18}\ eV$. Equivalent dose is also used when estimating the risk of biological effects from radiation exposure. Equivalent dose

denotes a weighting factor to different types of ionizing radiation and is measured in the SI unit sievert (Sv). For example, neutron radiation can cause 5 – 20 times more harm than exposure to an equivalent dose of beta radiation. The weighting factor for X-ray ionizing radiation is one, for the purposes of this discussion $1\ Sv = 1\ Gy$ [15, 16].

This exposure to ionizing radiation is a major challenge presented by CT X-ray medical and dental imaging. Exposure to ionizing radiation induces a risk of a variety of diseases and illnesses, including REIC, mental retardation, low-birthweight-infants, and tumors [17-19]. As more research is conducted, the evidence continues to suggest that these risks are stochastic. A stochastic risk means that there is no minimum threshold at which health effects due to exposure from radiation may occur. Furthermore, the risk that these diseases can occur increases linearly with exposure dose. This claim has been supported with evidence collected by research with Hiroshima and Nagasaki atomic bomb survivors, where an increasing rate of cancer was noted in linear association with increased exposure dose [18]. This no-threshold model on health risk associated with exposure to ionizing radiation is why the International Commission on Radiological Protections warns that we must make every effort to reduce exposure to the lowest possible limit [16].

This challenge presented by CT X-rays associated with dental imaging becomes more problematic when we consider the exposure dose cumulative with background dose. Humans are exposed to an annual background dose of radiation annually from multiple sources, including natural background radiation and man-made radiation. Studies suggest that the average person is exposed to a background dose of 2.4 mSv annually and that over three-quarters of man-made exposure sources are from medical imaging and nuclear medicine. Estimates from the most recent Biological Effects of Ionizing Radiation (BEIR) report claim that one out of a hundred

people will develop cancer due to a single annual exposure of 0.1 Sv above the radiation background dose [18]. This combination of background dose with exposure to ionizing radiation from medical imaging is a major concern. Studies suggest that roughly 2% of all invasive cancer incidents are attributable to X-ray radiation [20, 21].

Ionizing radiation also induces a variety of health risks excluding REIC. Hujoel et al. conducted a study linking low-birth-weight infants to dental radiography. A population of mothers exposed to 0.4 mGy of radiation during dental radiography was compared with a population of mothers with no known exposure. Results discovered an odds ratio (OR) for a low-birth-weight infant of 2.27 when the mothers were exposed to 0.4 mGy of radiation. An odds ratio compares the rates of disease in an exposed population to the rate of disease in an unexposed population. In this case, for every 1 low-birth-weight infant in the unexposed population, there were 2.27 low-birth-weight infants in the exposed population. The study included 29,000 women who had been exposed 40 weeks prior to the date of birth [17]. A study by Claus et al. focused on the risk of developing a meningioma (brain tumor) from radiation exposure during dental X-ray imaging. They found that over a lifetime, cases involving patients who had developed a meningioma were more than twice as likely to have taken a bite-wing examination (odds ratio:2.0) [19].

Despite these risks associated with exposure to ionizing radiation, Americans today are still exposed annually to significant levels of radiation during medical and dental imaging. An analysis of over 950,000 people from five health care markets across the United States found that medical imaging procedures lead to a cumulative effective dose that exceeds 20 mSv per year in 4 million Americans [22]. When we consider that the health risk of diseases increases linearly with exposure dose, and we consider the percentage of the population that is exposed during

routine medical and dental imaging, and we consider the cumulative annual exposure dose from medical imaging in combination with environment exposure, *the argument that any medical imaging exposure dose is well below a threshold at which disease might occur is faulted*. Exposing a large percentage of the population to ionizing radiation will increase the frequency of annual cancers in that population.

Indocyanine Green and Fluorescent Imaging

ICG is a fluorescent dye used for the visualization of cells and tissues for surgical imaging. ICG fluorescence is excited with infrared light between the wavelengths of $750 - 800$ nm, and longer emission wavelengths (up to 1700 nm) can be observed with an infrared camera [23]. As of this date, ICG is the only fluorescent dye approved by the Food and Drug Administration for surgical imaging. This is due to its low toxicity ($LD_{50} = 50 - 80 \frac{mg}{kg}$ for animals), rapid excretion into the bile, and the fact that small concentrations injected into a subject (around 5 mg/kg in rats) are visible [12, 24].

ICG is often used in the bio-medical sciences such as retinal angiography, cardiac output monitoring, and cancer surgical imaging due to its low cost, excellent signal to noise ratio, and real-time in-vivo imaging capabilities. When imaging with ICG, a long-pass filter is used in combination with the infrared camera, filtering the excitation signal and only imaging the emission signal. Only the target is imaged as the background is filtered by the long-pass filter, providing an excellent signal to noise ratio [24, 25].

NIR imaging is classified as NIR-I (700 – 900 nm) and NIR-II (1000 – 1700 nm). The advantages of NIR-II include an improved signal to noise ratio and deeper tissue penetration due to reduced photon absorption and scattering. However, NIR-II depends on more expensive InGaAs cameras as less expensive cameras, such as charge coupled devices, are generally not

sensitive to wavelengths below 1000 nm [23]. Current studies in dental imaging have used NIR-II for dental surgeries, imaging cracked teeth, and imaging caries; however, there have been very few or no other studies utilizing NIR-I to image the unerupted molar or impacted teeth [25].

NIR imaging with ICG also provides valuable advantages over conventional dental imaging methods such as CT X-ray and MRI. It does not expose the patient to any ionizing radiation and is not limited by special cases where specific localization of impacted teeth is required for correct diagnosis. NIR fluorescent imaging also provides the advantage of real-time *in-vivo* surgical imaging. In our studies, we have demonstrated ICG has a diverse imaging window beginning very shortly after ICG intradermal injection. We have also demonstrated that in-vivo images could be collected of molars via an endoscope from rats [12]. A separate study also demonstrated the feasibility of a hands-free NIR fluorescence imaging system for real-time image-guided surgery. The team demonstrated that the device could provide high detection sensitivity and signal-to-noise ratio in locating cancerous lesions and tumor margins [26].

Comparing Human and Rat Molars

The term dental morphology roughly refers to the shape and size of teeth. Teeth can be generally divided into two general components, a crown and a root. The crown is the visible portion of the tooth, erupting from the gum. The primary unit that makes up the crown is called a cusp, lobes that exhibit accessory ridges. The human molar consists of four cusps, the rat molar consists of two cusps. The crown is covered by the mostly inorganic enamel substance. Underlying the crown is the dentine, a substance more bone like. At the core of the tooth is the pulp, consisting of soft tissues and nerve vessels [27].

The first molars of mice and rats are often used in dental research. This is because of their rapid and similar development to the human molar. In mice, tooth crown development is

initiated postnatally and must establish a functional complex with its surrounding structures. This means the development of the first mouse molar is a valuable model of the human molar. The crown will complete formation by postnatal day 2 (P2). Root development begins at P4, and the root anchors into the jaw by P12. At P14 a clear eruption path has developed, and the tooth is ready to assume its functional position, although the molar is not completely developed until P16. At P20 the molar erupts [28].

2. Materials and Methods

NIR Dental Imaging System

An endoscopic NIR-I fluorescent imaging system was designed to test the potential of real time *in-vivo* dental imaging with ICG. The system includes a laser source (785 nm laser diode, Turnkey Raman Lasers-785 Series), a wide-field NIR camera (Guppy F038B; Allied Vision Technologies GmbH), two filtered lenses (low-pass lens: 785, band-pass lens: 800 nm) an endoscope (OSF-3; Olympus Corporation), a spectroscopic device (QEPro; Ocean Optics, Inc), a custom bifurcated fiber cable, and a computer [25].

To acquire *ex-vivo* wide-field and endoscopic images occlusal images, the Guppy F038B NIR camera was fixed ≈30 cm above the object of interest, and the OSF-3 endoscope was fixed ≈4 mm above the object of interest. Filters were used in order to optimize NIR detection, so that excitation NIR light and background light would not create noise. The custom designed bifurcated fiber cable was used to transmit the fluorescence excitation, and phases were compared with QEPro. A picture of the imaging system can be seen below in Figure 1. A diagram of the imaging system and its components can be seen below in Figure 2.

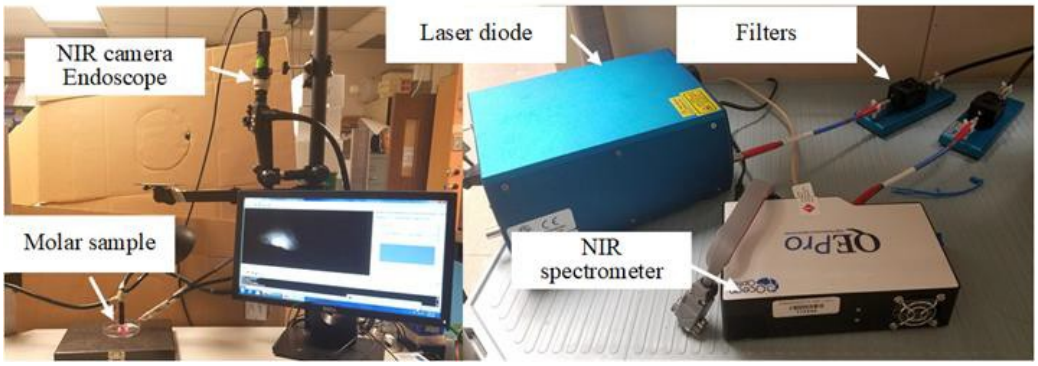

Figure 1. Picture of ICG NIR Imaging System

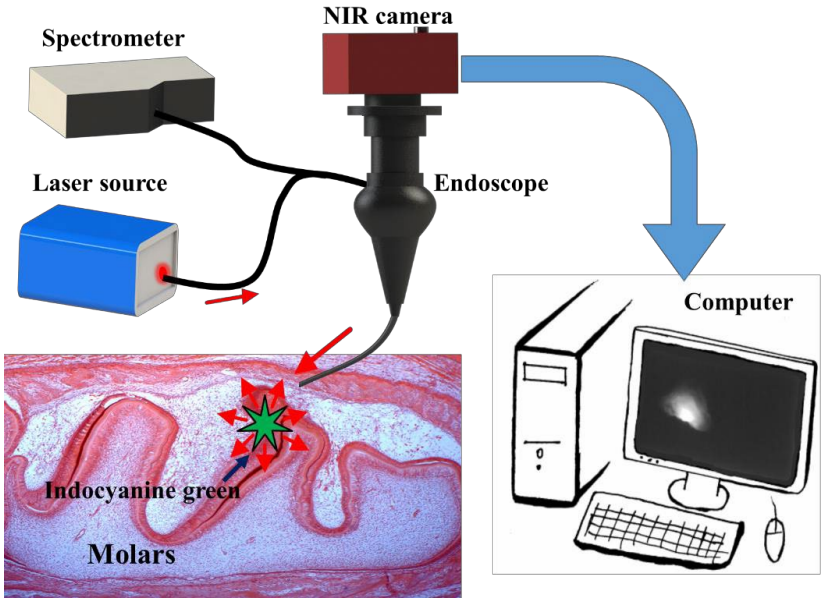

Figure 2. Drawing of ICG NIR Imaging System

Reagents and Animals

ICG powder, bovine serum albumin (BSA, 96%), and phosphate buffered saline (PBS) were purchased from Sigma-Aldrich (St. Louis, MO). The ICG powder (maximum solubility 1 mg/mL) was dissolved into ultrapure water (18.2 MΩ). BSA was dissolved into PBS to prepare a 4% BSA/PBS solution. ICG was diluted in the BSA concentration ranging from 1 fM to 1 μM to test the sensitivity of the imaging system.

Sprague-Dawley rats were bred in vivarium of the School of Veterinary Medicine, Louisiana State University. All experiments were approved by the Institutional Animal Care and Use Committee of the Louisiana State University (USA) and in accordance with the ethical guidelines for animal care.

Imaging Methods

Rats were administered 5mg/kg of the ICG solution per kg of body weight by intradermal injection in their backsides at P9, P14, and P31 days. In our most recent study, forty-four rats were euthanized before P14 so that unerupted molars could be imaged. The remainder were euthanized at P31 to image erupted molars. Rats were euthanized at 10 minutes, 4 hours, 24 hours, 48 hours, 72 hours, 120 hours, 144 hours, and 168 hours after injection. After the rats were euthanized, the mandibles were extracted, and the oral area was imaged using a wide-field camera and endoscope. We also imaged one euthanized rat with the endoscope *in-vivo,* before extracting the mandibles.

To compare the efficiency of the imaging system, we compared collected images to 2-D X-ray and CT imaging. The extracted mandibles of one P9 and one P14 rat were scanned by three-dimensional microCT (SANCO Medical AG, model μCT 40) using 55kV and 144 μA over 300 ms of exposure. The resolution of the images was 20 μm after reconstruction. The DICOM files were processed using Avizo Software Version 9.4.0 (Thermo Fisher Scientific).

To test the feasibility of the system in real world applications, we acquired human teeth and collected images on the human teeth. We submerged the human teeth in our ICG solution for 24 hours, then immediately took NIR images with the imaging system. Our goal was to identify oral diseases such as caries and cracks, as well as observe morphology such as the enamel and dentin.

Imaging Windows

We developed a parameter named intensity-mean difference (IMD) to quantitatively evaluate the imaging contrast of the imaging system and its imaging window. The parameter is calculated by taking the difference between the fluorescent intensity of the pixels between the

molar region and the lingual background. A one-pixel wide by 20 to 40 pixels long area was selected across the molar and lingual regions, similar to a line-segment or queue of pixels, fluorescent intensity in gray scale values were compared between each point in the queues. The queues were collected through the lingual and molar regions and were parallel to each other. Figure 3. below shows the location of the queues in the molar and lingual regions.

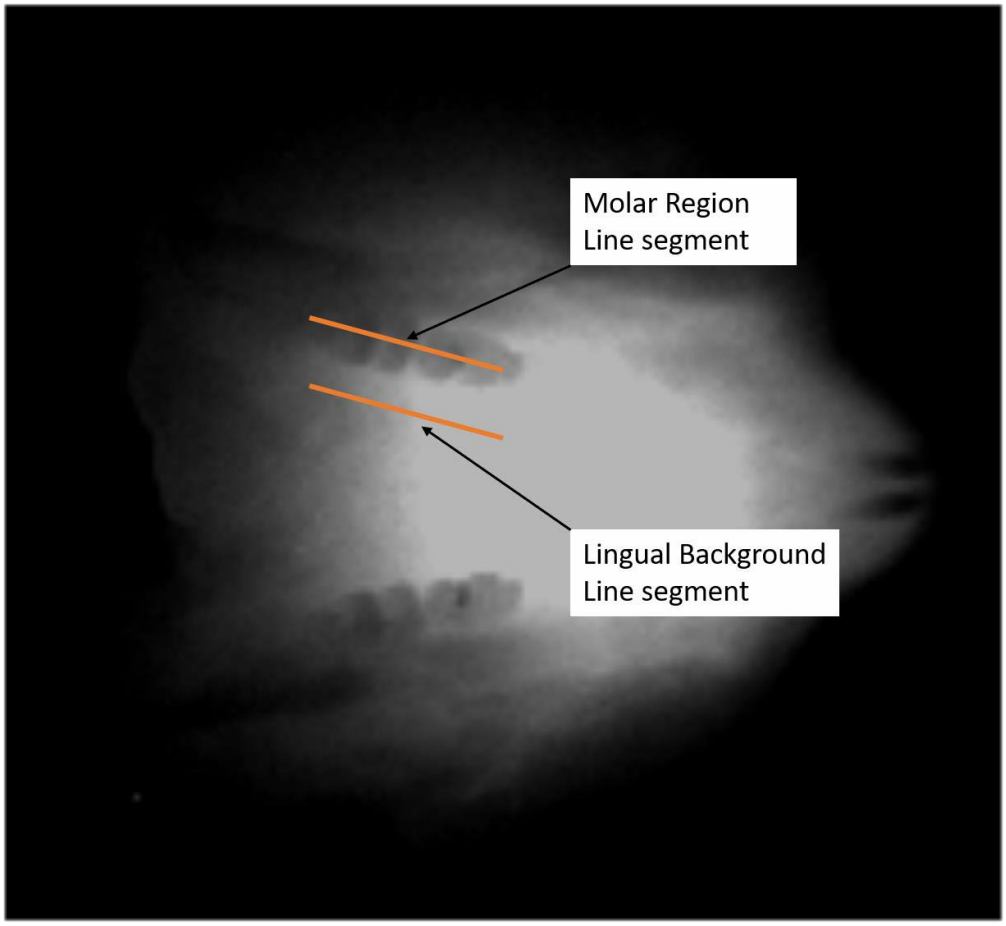

Figure 3. Pixels creating line segments to define IMD value for each rat

Because the NIR image collected with the imaging system is black and white, the image can be considered a gray scale image and each pixel can be considered a shade of gray. We used gray-scale values to measure the intensity of the fluorescent light. Gray-scale values are an 8-bit integer ranging from 0 to 255 and are often used in image processing techniques. Generally, 0

represents totally black and 255 represents totally white. Because gray-scale values are a discrete binary integer, they are unitless. We compared the difference between gray-scale value in the first pixel of the queue from the lingual background to the first pixels from the queue in the molar region, then continued respectively to the second, and third, from i = 0 until i = n as in Equation 1.

$$D_{mean\_diff} = avg(\sum_{i=0}^{i=n}(g_m - g_b))$$

Equation 1.

Where g_m and g_b are the greyscale values of each individual pixel in the queues of the molar and lingual regions and n is the number of pixels in the measured queues from the image. These IMD values provide an objective value to measure the contrast of the imaging system.

We were also curious to see if we could image molars after laser ablation treatment of the dental follicle. One P14 rat had its left molars treated via laser ablation in order to cause molar eruption inhibition. Dental follicle was treated with a 0.6 W laser (Picasso Life, AMD GROUP LLC, USA) over a period of 5 seconds. Only the left molar was treated, leaving the right molar as a control. After treatment, images were collected via the Guppy F038B wide field camera.

3. Results

General Concept of NIR dental imaging

Lab rats were injected with ICG, mandibles were extracted, and our NIR imaging system successfully imaged the molar regions via wide-field and endoscopic imaging. Molar regions could clearly be detected via wide-field imaging, and crown and cusp details could be observed via endoscopic images. Both erupted and non-erupted molars could be identified with our imaging systems wide-field view, and crowns and cusps could be clearly observed in erupted and non-erupted molars with endoscopic images.

Figure 4. below is a collection of NIR images collected by our system of a P21 rat's erupted molars 4 hours after intradermal injection. Figure 4. (A) displays a drawing of a rat mandible, the drawing displays the location of the rats first and second molars (M1 and M2), as well as the three crowns on M1, and the two crowns on M2. Figure 4. (B) is an *ex-vivo* wide field NIR occlusal image of a P21 rat's extracted mandibles. Wide-field imaging clearly identified the molar regions, and the first and second molars could be distinguished. Figure 4. (C) is an *ex-vivo* occlusal NIR endoscopic image of the same P21 rat's extracted mandible. Endoscopic imaging was able to capture details of crowns, lingual cusps, and buccal cusps.

Figure 5. shows bright field microscopy, bright field endoscopy, NIR wide-field, and NIR endoscopy images of an extracted P9 rat mandible. At P9, rat molars are unerupted and not fully developed. Figure 5. (A & B) displays a bright-field occlusal image of extracted rat mandibles. We included bright-field images to give an example of a standard visual dental examination. The unerupted molar regions can be identified with the naked eye, but very little information on the overall dental morphology can be gathered. Figure 5. (C & D) shows wide-field and endoscopic NIR images taken with our system. The molar regions are not as easily

distinguishable as with the P21 rat, since molar development was not fully complete. However, the fully developed crowns of the first molar could still be identified with endoscopic images for both left molars (LM) and right molars (RM).

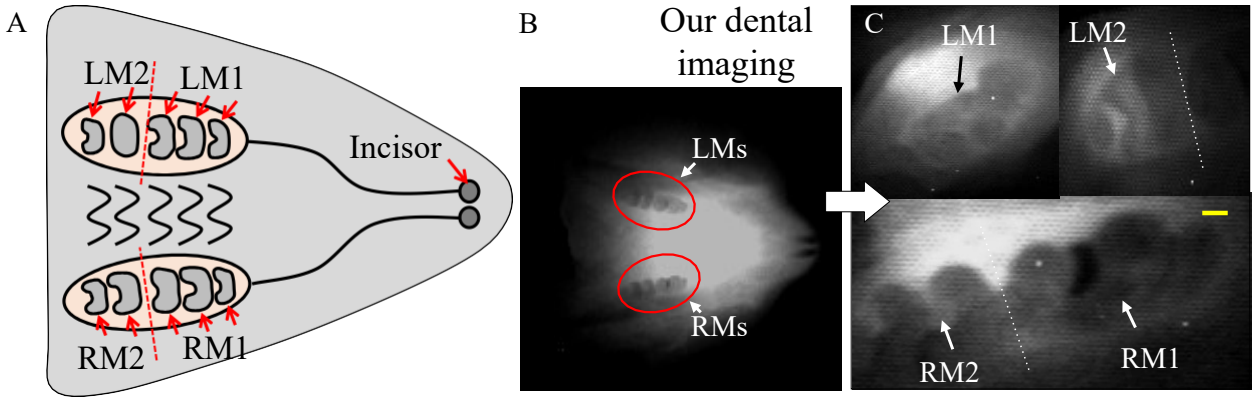

Figure 4. (A) dental structures (not to scale), e.g. molars (B) wide-field occlusal view; (C) endoscopic images. Yellow bar: scale bar, 1 mm.

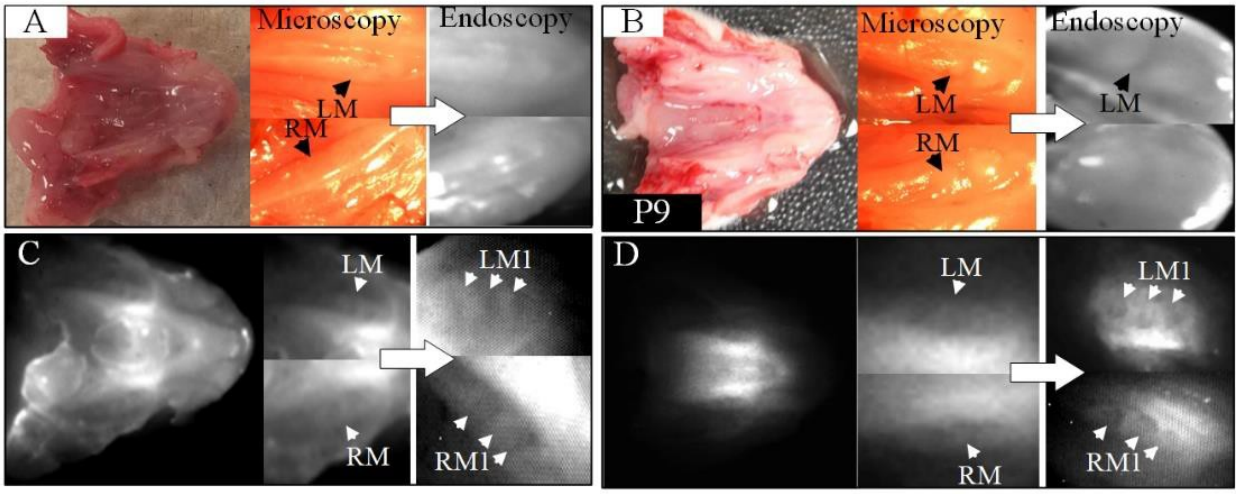

Figure 5. (A & B) bright field and (C&D) NIR microscopy and endoscopy of P9 extracted rat mandibles.

Optimization of NIR Imaging Windows

We aimed to discover an optimized length of time after ICG injection to optimize imaging contrast. This optimized imaging window gives an idea as to how soon a dentist could image molars and as to how long after injection morphology could be observed. Figure 6. below

shows NIR images of a 3 different rat molar regions (MR) and the surround lingual background (LB) and buccal background (BB). Figure 6. (a & b) displays a P9 rat's unerupted molars, (c & d) displays a P14 rat's unerupted molars, and (e & f) displays a P31 rat's erupted molars. Also included in the image is the fluorescent intensity at those points measured in grayscale values; we added a yellow bar to pinpoint the pixels at which fluorescent intensity was measured. We found that during the first 24 hours, the fluorescent intensity of the lingual background was often higher than that of the molar region. From this discovery we chose the difference between LB from the MR to define our IMD values.

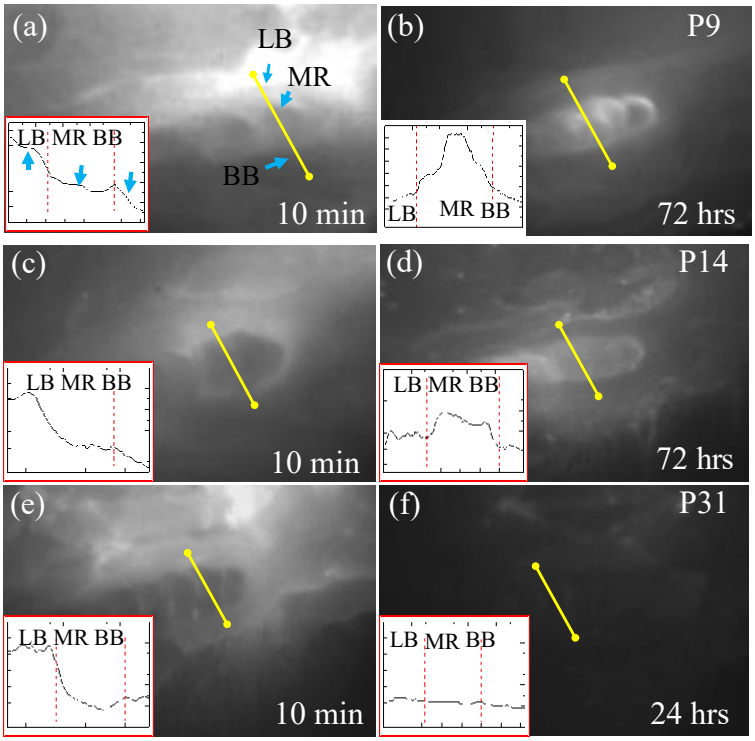

Figure 6. Fluorescent intensity of lingual, buccal, and molar regions. (a & b) P9 rat unerupted molars, (c &d) P14 rat unerupted molars, (e & f) P21 rat erupted molars. [12]

The average fluorescent intensity was measured from the molar and lingual regions for

each rat using the spectrometer as described above, and the data was organized in Figure 7. below. Fluorescent intensity was measured in grayscale values, and the difference between LB

intensity and MR intensity was defined as IMD. The x-axis represents the time after intradermal injection in minutes or hours at which rats were euthanized and imaged, while the y-axis represents unitless gray scale values. Also included in Figure 7. is the standard deviation of the difference measured in each pixel across the lingual and molar regions. There was one outlier in the standard deviation for a P31 rat imaged after 120 hours. This was due to a single bright white spot in the molar region which we assumed was food.

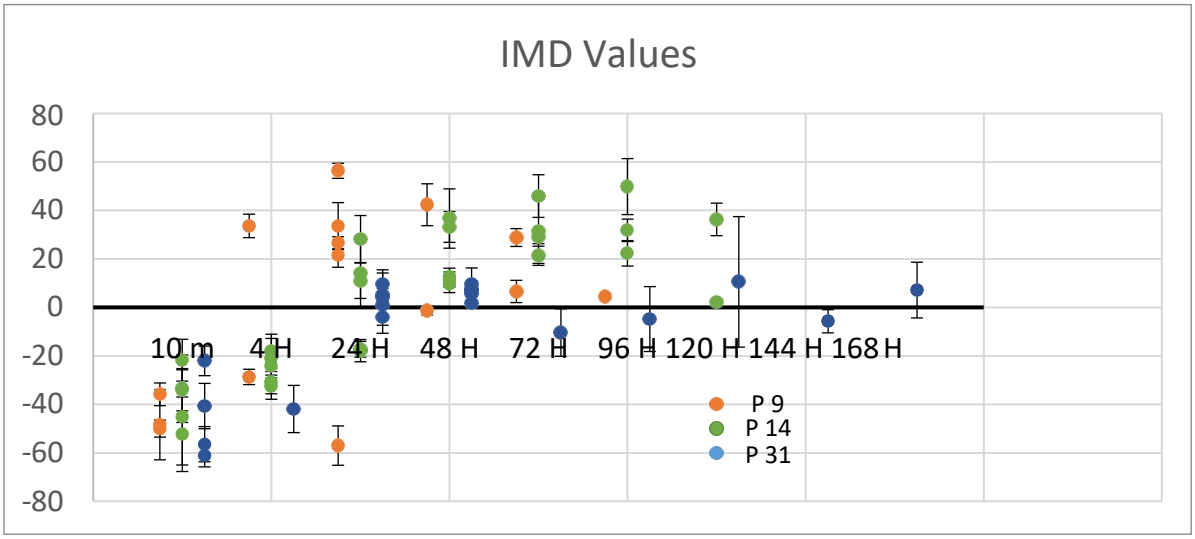

Figure 7. IMD values

Significant IMD values could be measured no later than 10 minutes for all rats. For P31 rats with erupted molars large IMD values were measured up to 24 hours after injection, however after 24 hours the difference declined to small numbers. For P9 and P14 rats with unerupted molars, large IMD values were measured up to 120 hours after injection.

An interesting discovery was that for P9 and P14 rats IMD values were negative during the first 24 hours, but positive later in the imaging windows. The fluorescent intensity in the molar regions increased as time passed, and the intensity of the lingual background decreased.

NIR and X-ray Comparison

Our next objective was to test the systems wide-field endoscopic imaging capabilities and compare them with bright-field, 2-D X-ray, and 3-D CT images. Figure 8. below shows (a) a wide-field NIR image, (b) an endoscopic NIR image, (c) an endoscopic bright-field image, (d) a 2-D X-ray image, and (e & f) a 3-D CT X-ray image of unerupted molars from the extracted mandibles of a P9 rat.

CT X-ray imaged both soft dental follicle tissues, and clear morphology of crowns and cusps for both molars as shown in Figure 8. (e &f). In Figure 8. (f) the molar regions are obscured by the dental follicle soft tissues, but clear morphology of the molars, crowns, and cusps could be observed by adjusting the micro CT software's (Avizo) colormap feature. Figure 8. (d) displays 2-D X-Ray radiographic images. Similar results were achieved as a CT image, however there was some super-imposition around the left molars. We believe this happened because the molars were not perfectly perpendicular with the x-y plane as the occlusal image was scanned. Although the image is clear, the cusps are not as clearly observed in 2-D X-ray as with CT imaging. These X-ray images were taken in our lab with our own equipment.

We compared these X-ray images to images collected with our imaging system. Molar regions for P9 rats were not as easily identifiable with wide-field imaging, but the first molar region could still be observed as in Figure 8. (a). Molar 1 crowns and cusps could be identified and observed using the endoscope as in Figure 8. (b), and we compared this image to a bright-field endoscope image under the same conditions in Figure 8. (c).

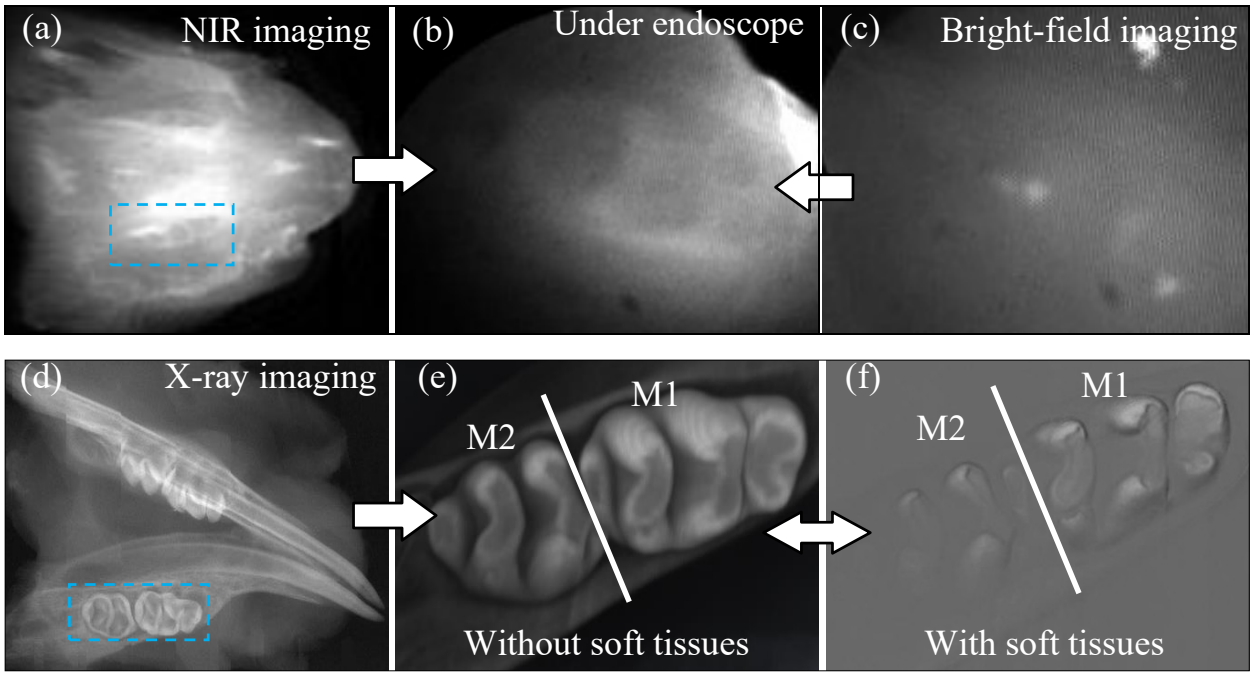

Figure 8. Unerupted molar (a) NIR wide-field image, (b) NIR endoscope image, (c) endoscope brightfield image, (d) 2-D X-ray, (e) CT with soft tissue (f) CT without soft tissue [12]

Figure 9. below shows NIR *in-vivo* NIR and CT images of a P14 rat's unerupted molar regions. In this case, mandibles were not extracted before NIR imaging. Figure 9. (d) displays a CT occlusal image, and Figure 9. (e) displays a CT periapical images of the P14 rat's mandibles. Figure 9. (b) is a wide-field NIR *in-vivo* occlusal image and Figure 9. (c1 & c2) are *in-vivo* NIR endoscopic images of the same rat. The endoscope was inserted into the oral cavity of the euthanized rat for endoscopic imaging. *The oral cavity of the imaged rat was roughly 5mL*. For the P14 rat, both the first and second molar regions could be identified with wide-field NIR images. The endoscopic images were more difficult to interpret due to the small oral cavity of the P14 rat, however lingual cusps could still be identified.

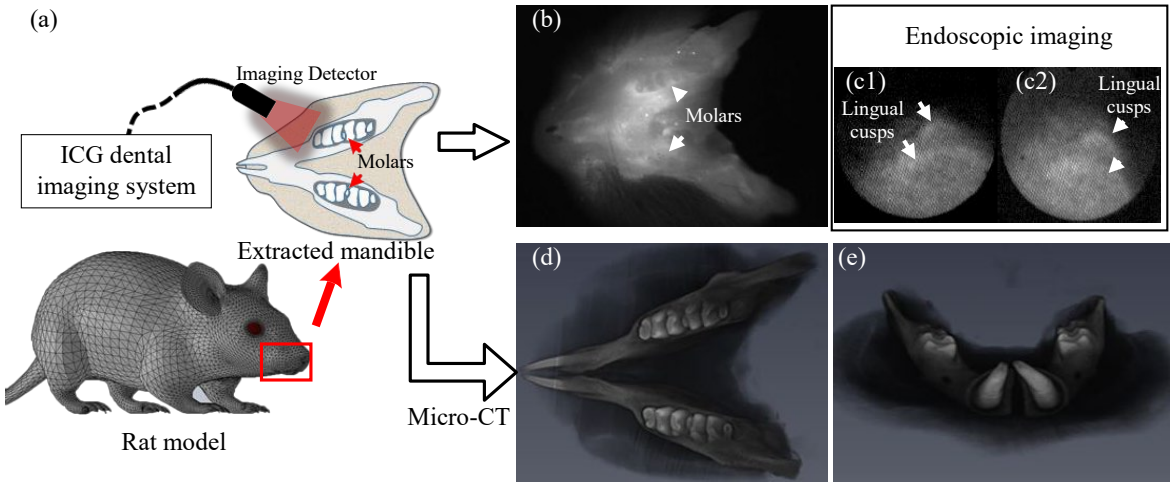

Figure 9. P14 rat *in-vivo* unerupted molar (a) system configuration (b) occlusal wide-field image, (c) endoscopic image, (d) CT occlusal X-ray, (e) bitewing CT X-ray [12]

Imaging Laser-Treated Molars

The imaging system was able to identify differences between laser ablation treated and control molars for both erupted and non-erupted molars. Figure 10. below shows a drawing of how laser ablation treatment was conducted, bright-field images of treated and control unerupted molars, and NIR wide-field images of unerupted molars from extracted P9 rat mandibles. From the bright-field images, we can see the treatment successfully inhibited the eruption of the treated molar. From the wide-field NIR imaging, we can once again clearly identify the molar regions. Changes in the morphology of the treated molar were observed. We aim to research taking advantage of this difference in future research.

We further tested the system imaging a P31 rat's erupted molars. Left molars were treated via laser ablation and right molars were left as a control. Figure 11. below shows bright-field and endoscopic NIR images of the rat's treated and control molars. Figure 11. (a & c) show bright-field images of treated and control molars respectively, where Figure 11. (b & d) show

endoscopic NIR images of treated and control molars. As expected, endoscopic imaging identified clear morphology of lingual and buccal cusps of each crown on the first molar.

Endoscopic imaging was able to further notice changes in the treated molar as well. Morphology had been slightly altered and cusps could not be as sharply identified due to changes in dental structure during treatment.

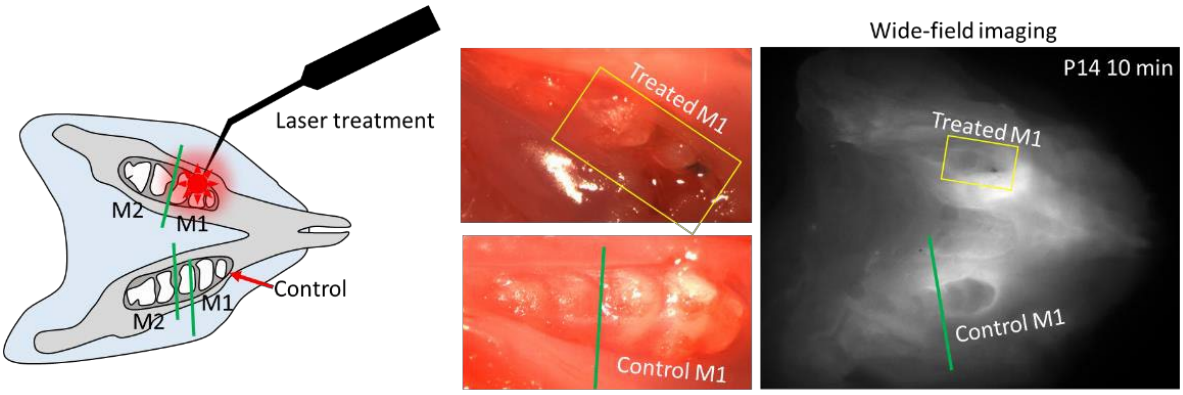

Figure10. Drawing of treatment, wide-field bright-field images of unerupted molars, NIR wide-field NIR images of treated and control molar

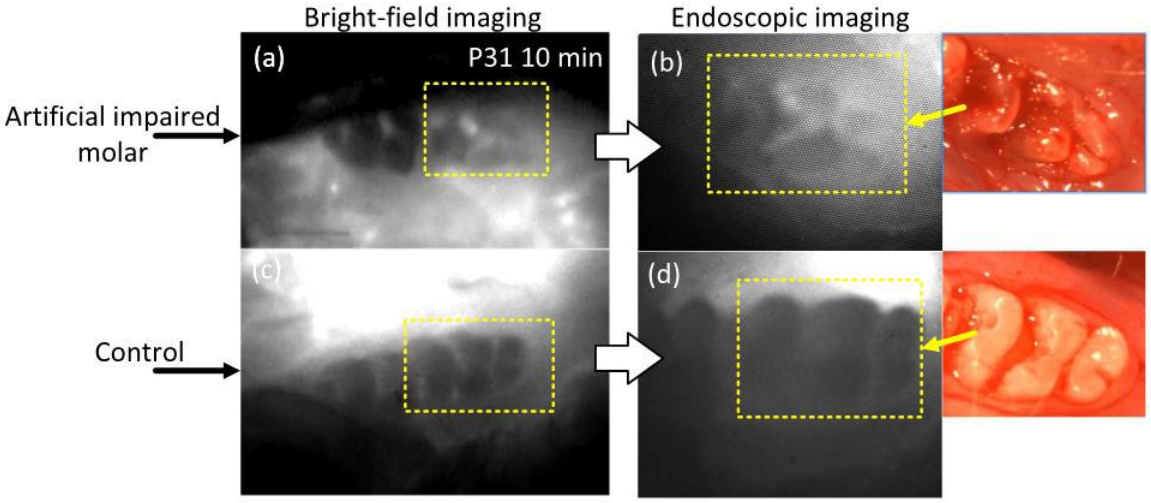

Figure 11. (a) bright-field image of treated molar, (b) endoscopic NIR image of treated molar, (c) bright-field image of control molar, (d) endoscopic NIR and bright-field images of control molar with normal eruption, [12]

Imaging Human teeth

We then tested our imaging system on human teeth. Human teeth were obtained and submerged in the ICG solution, and NIR imaging was performed. A human tooth was

submerged for 24 hours and then imaged, and then immediately imaged via wide-field spectrometry. Figure 12. below shows the results alongside a drawing of the human tooth and the tooth before submergence. NIR-I light successfully propagated through the human tooth, and enamel and dentin could be observed from the collected image.

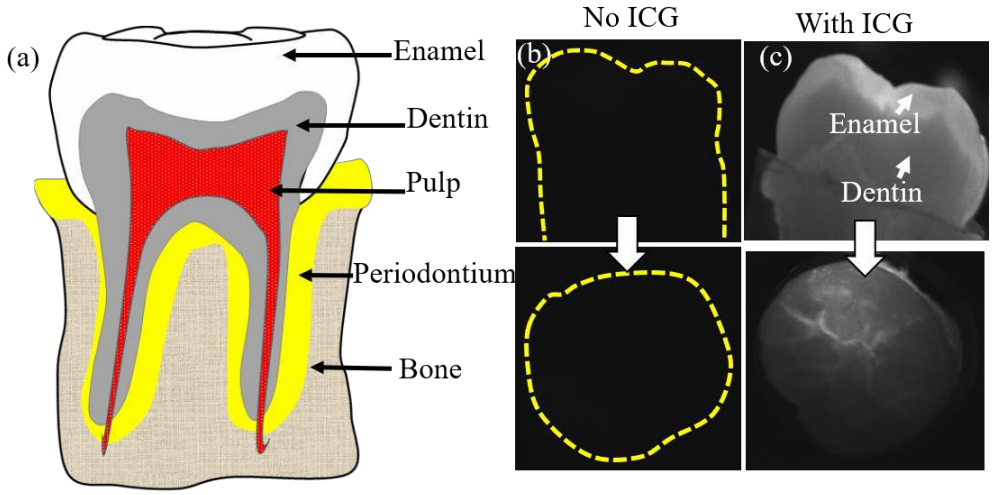

Figure 12. (a) drawing of human tooth (b & c) NIR images of human tooth before and after submergence in ICG

4. Discussion

The objective of this research is to test the feasibility of wide-field and endoscopic NIR ICG dental imaging and compare it to current methods available today, mainly X-ray. To accomplish this, we developed a NIR imaging system, imaged erupted and unerupted rat molars, directly compared our NIR images with X-ray, developed an imaging window at which ICG dental imaging can be conducted, imaged human teeth, and tested our system on treated unerupted molars.

We are the first pioneers in developing an ICG NIR-I imaging system for dental imaging purposes. Our aim is to develop a system that is safe, effective, does not require extensive training to use, is portable, affordable, and can be used for a variety imaging needs. We developed a system and tested its capability to meet these requirements in experiments [12, 25]. We used NIR-I because most studies rely on NIR-II, even though a far less expensive system could be developed with NIR-I. A NIR I camera is far less expensive than a NIR II camera. NIR I images can be captured with a CCD or a CMOS-based camera which can be purchased for around $400, whereas NIR II requires InGaAs which will cost at least $8000 [29]. We also used NIR I because there has been no other research published with such a system [25], and we were curious to test it.

We tested our imaging system on rat molars due the fact that the first molars of the rat have similar morphology compared to human molars, particularly the first molar. We tested our system on P9, P14, and P21 rats. Testing the system on P9 rats was used to identify the system's efficiency imaging molars that were under-developed since the molar is not completely developed until P16. Testing the system on P14 rats was used to identify the systems efficiency

imaging unerupted molars that were prepared to erupt. Testing the system on P21 rats was used to identify the system's efficiency imaging erupted molars.

Our results show that NIR-I can be utilized to image molar morphology and surrounding structures for both erupted and unerupted molars. Figure 4. shows images taken of a P21 rats erupted molars. We could clearly identify the first and second molars, as well as examine individual crowns and cusps. The fact that these images were taken 4 hours after intradermal injection suggest that there could be practical use for the system in real-world scenarios. Un-developed rat molars could also be imaged by NIR-I. Figure 5. shows images of P9 rat molars. The first molars of a rat are not fully developed until P16, but the imaging system could still identify the first molar region via a wide-field NIR camera and cusp could be identified via an endoscope. We further tested the experiment in-vivo on a P14 rat. A P14, rat molars are mostly developed and are ready to erupt. The molar regions and surrounding hard tissues could be identified via the wide-field NIR camera. Lingual cusps could be identified by inserting the endoscope into the 5 ml oral cavity of the mouse as seen in Figure 9. (c1 & c2).

In Figure 8. and figure 9. we compared rat P9 and P14 molars to 2-D and 3-D CT X-ray. X-ray technology is generally considered to be the gold-standard for contrast in medical imaging, although there are several associated challenges including health, time, and financial cost [30]. As expected, a high imaging contrast was obtained from the X-ray imaging. Clear morphology of the buccal and lingual cusps could be observed, and surrounding hard tissues were easily identified. The NIR images collected on unerupted molars are not as clear as the images collected via X-ray; however, the molar region could still be identified for the unerupted molar via wide-field imaging, and details of the crown and cusps could be observed via endoscopic imaging. Also, hard and soft tissue could be identified by their difference in fluoresce intensity.

If our imaging system can successfully image the unerupted molar without any of the health risk associated with X-ray technology, we believe this system can be a solution to the challenge presented by exposing two thirds of the population to ionizing radiation through dental imaging. The biggest advantage in our fluorescence imaging system is that it offers real-time imaging that X-ray technology does not. In the future, a dentist could use an endoscope to take dental images as he operates as seen in image Figure 9. (c1 & c2). Other advantages of our system over X-ray is that there is no super-imposition, as seen in figure 8 (d).

We further investigated the optimized imaging windows with the NIR system. Imaging with ICG in other fields such as cancer and lymph node detection have an imaging window of 3 hours at best [31, 32], but our imaging window has a minimum of 24 hours for both erupted and unerupted molars, and a maximum imaging window of up to 120 hours for the unerupted molar (see Figure 7.). The imaging window began no later than 10 minutes after intradermal injection and lasted up to 120 hours after the application. This window could be of great practical use to dentists. Images could hypothetically be taken no later than 10 minutes after a patient walks into the office, and images could continue to be taken days later without any re-application of the ICG.

The second exciting discovery from studying the imaging windows was that the molar regions often increased fluorescent intensity whereas the buccal and lingual background diminished in intensity after 42 hours. As seen in Figure 7. the difference in fluorescent intensity between the lingual and molar regions was negative during the first 24 hours, then becomes positive. We aim to explore further into the phenomenon, as this could be useful deciphering NIR images and possibly identifying different types of tissues.

We were also able to image molars after the dental follicle was treated with laser ablation. The image of the inhibited molar was “blurred” due to damage around the dental follicle. There were clear differences between the images of unerupted molar and control molars as seen in Figure 10. Further differences were noted between the fully erupted molar and the partially erupted molar as seen in Figure 11.

Finally, we tested ICG imaging on the human tooth. As seen in figure 12. dentin and enamel could be observed via NIR imaging after submerging the tooth in an ICG solution for 24 hours. The most exciting aspect of these results is that images were collected without intradermal injection, only submergence. In the future, dental images could be taken after a patient rinses with an ICG base mouthwash. Most studies rely on NIR-II to image human teeth for cracks and caries [24]. We aim to conduct future research in screening for caries with our NIR-I system. If NIR-I fluorescent imaging could accurately detect hidden caries, especially hidden caries, it would provide a less expensive and safer alternative to bite-wing X-ray.

Our research shows that there is potential for NIR-I to image general morphology and surrounding hard tissues inside the oral region. However, in the future we must demonstrate that NIR imaging can be utilized for a broader set of imaging purposes. Before extracting molars surgically, dentists need visual information for a variety of different tissues, such as soft tissues and nerve vessels [6]. There have been some other instance of imaging soft tissues such as pulp using fourier transform infrared imaging [33]. We included a spectrometer in our system to measure fluorescent intensity levels. If we could utilize the spectrometer to identify different tissues, it would be an exciting discovery. Also, further research must be done to test the system’s ability to detect hidden caries.

5. Conclusion

The studies conducted provide a proof-of-concept that ICG I NIR fluorescent imaging can be utilized to image both erupted and nonerupted molars. Although the results are not as superb as CT X-ray imaging, we are confident that our imaging system can provide dentists the capability to screen and treat a variety of oral diseases without exposing the patient to ionizing radiation. The system also has potential to provide real-time *in-vivo* images, which is not something CT X-ray can accomplish.

The imaging system we have developed is also less expensive and more portable than other methods available today. We have demonstrated that NIR I can efficiently image rat molars and provide a cheaper solution than using a NIR II camera. The 1-2 cm tissue penetration of NIR I is enough to image the unerupted molar.

In the future, we will need to prove the system can do three things. First, it needs to be able to distinguish between hard and soft tissues. Second, it needs to be able to accurately detect hidden caries. And finally, we must demonstrate its use in clinical trials.

Citations

1. Sheiham, A., et al., *Oral health, general health and quality of life*. 2005, SciELO Public Health.

2. Yap, A., et al. *Oral Health Equals Total Health: A Brief Review.* Journal of Dentistry Indonesia, 2017. **24**(2): p. 59-62.

3. *Oral health in America: a report of the Surgeon General.* 2000, NIH publication. p. 155-188.

4. Kassebaum, N.J., et al., *Global burden of untreated caries: a systematic review and metaregression.* J Dent Res, 2015. **94**(5): p. 650-8.

5. Trevisan, T.C., et al., *Hidden caries: A critical review.* Scientific Journal of Dentistry, 2015. **2**: p. 33-36.

6. Santosh, P., *Impacted mandibular third molars: review of literature and a proposal of a combined clinical and radiological classification.* 2015. **5**: p. 229-234.

7. Association, A.D., *Dental radiographic examinations: recommendations for patient selection and limiting radiation exposure.* Chicago: ADA, 2012.

8. Metsala, E., A. Henner, and M. Ekholm, *Quality assurance in digital dental imaging: a systematic review.* Acta Odontol Scand, 2014. **72**(5): p. 362-71.

9. Vandenberghe, B., R. Jacobs, and H. Bosmans, *Modern dental imaging: a review of the current technology and clinical applications in dental practice.* Eur Radiol, 2010. **20**(11): p. 2637-55.

10. Shah, N., et al. *Recent advances in imaging technologies in dentistry.* World J Radiol, 2014. **6**(10): p. 794-807.

11. Tymofiyeva, O., et al., *Three-dimensional localization of impacted teeth using magnetic resonance imaging.* Clin Oral Investig, 2010. **14**(2): p. 169-76.

12. Zhongqiang Li, , et al. *Indocyanine green-assisted near infrared dental imaging and its optimized imaging window using rat as the animal model.* 2018.

13. Ionizing radiation. *https://www.who.int/ionizing_radiation/about/what_is_ir/en/* [cited 2018 12/12].

14. Ionizing Radiation *http://chemed.chem.purdue.edu/genchem/topicreview/bp/ch23/radiation.php* [cited 2018 10/15].

15. Ionizing Radiation *https://www.who.int/ionizing_radiation/about/what_is_ir/en/index2.html* [cited 2018 12/12].

16. *Annals of the ICRP*, 2012, ELSEVIER.

17. Hujoel, P.P., et al. *Antepartum Dental Radiography and Infant Low Birth Weight.* American Medical Association, 1987. **291**.

18. Council, N.R., *Health risks from exposure to low levels of ionizing radiation: BEIR VII phase 2*, N.A. Press, Editor. 2006.

19. Claus, E.B., et al. *Dental x-rays and risk of meningioma.* Cancer, 2012. **118.18**: p. 4530-4537.

20. Lin, E.C. *Radiation risk from medical imaging*. in *Mayo Clinic Proceedings*. 2010. Elsevier.

21. de González, A.B., et al., *Projected cancer risks from computed tomographic scans performed in the United States in 2007.* Archives of Internal Medicine, 2009. **169**(22): p. 2071-2077.

22. Fazel, R., et al. *Exposure to Low-Dose Ionizing Radiation from Medical Imaging Procedures.* The New England Journal of Medicine, 2009.

23. Starosolski, Z., et al., *Indocyanine green fluorescence in second near-infrared (NIR-II) window.* PloS one, 2017. **12**(11): p. e0187563.

24. Alander, J.T., et al., *A review of indocyanine green fluorescent imaging in surgery.* Int J Biomed Imaging, 2012. **2012**: p. 940585.

25. Li, Z., et al., *Endoscopic near-infrared dental imaging with indocyanine green: a pilot study.* Ann N Y Acad Sci, 2018. **1421**(1): p. 88-96.

26. Liu, Y, et al. *Hands-free, wireless goggles for near-infrared fluorescence and real-time image-guided surgery.* Surgery, 2011. **149.5**: p. 689-698.

27. Katzenberg, A.G., et al. *Biological anthropology of the human skeleton*, ed. J.W. Sons. 2018.

28. Lungova, V., et al., *Tooth-bone morphogenesis during postnatal stages of mouse first molar development.* J Anat, 2011. **218**(6): p. 699-716.

29. Zhongqiang Li, W.Z., Alexandra Ramos, Michelle L. Osborn, Shaomian Yao, Jian Xu, *Evaluation of indocyanine green-assisted near-infrared dental imaging and its comparison to the near-infrared-II imaging.*

30. Santos Junior, V.E.D., et al., *Are there hidden caries or is this another limitation of the diagnostic conventional exams.* Revista Odonto Ciência, 2015. **30**(2): p. 45.

31. Yokoyama, J., et al., *A feasibility study of NIR fluorescent image-guided surgery in head and neck cancer based on the assessment of optimum surgical time as revealed through dynamic imaging.* Onco Targets Ther, 2013. **6**: p. 325-30.

32. Fujiwara, M., et al., *Sentinel lymph node detection in skin cancer patients using real-time fluorescence navigation with indocyanine green: preliminary experience.* J Plast Reconstr Aesthet Surg, 2009. **62**(10): p. e373-8.

33. Giorgini, E., et al. *Fourier Transform Infrared Imaging analysis of dental pulp inflammatory diseases.* Oral Diesease 2017. **23**(484-491).

Vita

Thomas Hartzler, born in Biloxi, Mississippi, graduated from St. Mary's high school in Stockton, California before earning his Bachelor of Science in Electrical Engineering from Mississippi State University. Before earning his Master of Science in Electrical Engineering at Louisiana State University, he worked in relay controls and automations. He hopes to use his learned skills working in bio-medical research to pursue a people-focused career.